





Investigation of the Nanomechanical Properties of Crystalline Anatase Titanium Dioxide Films Synthesized Using Atomic Layer Deposition

Y.S. MOHAMMED,^{1,2} K. ZHANG,^{2,3} P. LIN,^{2,3} H. BAUMGART ^{2,3}
and A.A. ELMUSTAFA ^{1,2,4}

1.—Department of Mechanical and Aerospace Engineering, Old Dominion University, Norfolk, VA 23529, USA. 2.—Applied Research Center, Thomas Jefferson Lab, Newport News, VA 23606, USA. 3.—Department of Electrical and Computer Engineering, Old Dominion University, Norfolk, VA 23529, USA. 4.—e-mail: aelmusta@odu.edu

Crystalline titanium dioxide (TiO₂) polycrystalline films of 500 nm thickness were synthesized using atomic layer deposition (ALD) on p-type Si (100) substrates. The crystal structure, phase purity, film thickness and morphology were characterized using x-ray diffraction (XRD), field emission scanning electron microscopy (FE-SEM) and atomic force microscopy (AFM). The nanomechanical properties were measured using nanoindentation. Due to low temperature ALD deposition, XRD revealed a single anatase phase growth. FE-SEM images indicate columnar grain structure growth primarily in the vertical directions. The hardness was measured as 5 GPa at 24% film thickness, which is considerably softer compared to the reported benchmark values of the well-known rutile phase of ~ 12 GPa. The elastic moduli were estimated as 138 and 145 GPa for samples A and B, respectively. Samples A and B are identical except that sample A is slightly thicker; the slight difference in thickness has no influence on the results.

INTRODUCTION

Titanium dioxide (TiO₂) thin films have found their way into a plethora of applications and have enjoyed renowned attention. TiO₂ films are used in artificial heart valves because of their superb biocompatibility.¹ They are also used in heterogeneous catalysis as a corrosion-protective coating² and as electrode material in lithium rechargeable batteries. The photocatalytic activity of TiO₂ is exhibited in both the anatase and the rutile phases. Self-cleaning windows have been created by harnessing the photocatalytic properties of TiO₂ coatings on glass. Hydroxyl radicals are generated upon exposure to ultraviolet light, which breaks down organic dirt on windows and simultaneously enhances

hydrophilicity. Likewise, the photocatalytic properties of TiO₂ thin films are manifest in medical applications such as bactericidal coatings of wound care gauze and surgical instruments. Investigating the effect of Sn content on the structural and photoelectrochemical properties of TiO₂ nanostructure, Kumar et al. concluded that 3 at.% Sn doping impeded the formation of anatase structure and helped the formation of the rutile structure.³ In their study, the hydrophilic TiO₂ nanostructure was grown by the sol-gel process.³ Mansoor et al. investigated the photoelectrochemical properties of Mn₂O₃-TiO₂ composite thin films fabricated using aerosol-assisted chemical vapor deposition (AACVD) at different temperatures. They concluded, among the various thin films investigated, the thin film deposited at 500°C showed better porous and textural morphology with a direct band gap of 2.75 eV and a photocurrent density of 1.3 mA cm⁻² at 0.7 V vs Ag/AgCl/3 M KCL using 0.5 M aqueous solution of Na₂SO₄ as the electrolyte.⁴ Although historically the chemical industry

(Received April 24, 2020; accepted August 21, 2020; published online September 8, 2020)

has been using huge amounts of rutile phase TiO_2 in paints, plastics, paper, food and cosmetics, in a powder form, thin films of TiO_2 have recently emerged in many other applications. Fabrication of TiO_2 films has intensified in the last 2 decades because of their notable optical and electronic properties^{5–8} and their excellent potential applications for gas sensing. Polycrystalline TiO_2 films exhibit good sensing performance for CO , H_2 , ethanol and methane gases.^{9–13} Recently, Sennik et al. reported that anatase TiO_2 thin films yielded a better gas sensing ability to H_2 , which is attributed to the dominant (101) facets of anatase.¹⁴ Another application for anatase TiO_2 was reported by Etgar et al. when they realized that impressive photovoltaic performance was noted with perovskite/ TiO_2 heterojunction solar cells, which were fabricated using pure anatase phase TiO_2 nanosheets with dominant (101) facets serving as the electron collector.¹⁵

Literature reports indicate that TiO_2 thin films exist in three different crystalline phases: rutile and anatase, which are both tetragonal, and brookite, which is orthorhombic.^{16–19} Rutile is generally formed at temperatures $> 600^\circ\text{C}$ and is the most thermodynamically stable polymorph of TiO_2 . It is also considered the most common form of TiO_2 found in nature. On the other hand, the anatase phase is recognized to be less stable.¹⁹ Amorphous TiO_2 films are routinely produced when the substrate temperature during deposition is very low, typically below the recrystallization temperature of TiO_2 .^{19–22} In their 2007 study, Wojcieszak et al. concluded that the anatase phase TiO_2 consists of preferentially (101) and (200) oriented lattice planes with an average crystallite size of 26 nm, which result from deposition of TiO_2 thin films by a conventional magnetron sputtering process.¹⁸ Alimirsalari et al. synthesized TiO_2 nanosheets to be used in solar cell devices that do not require large surface areas, such as colloidal quantum dot and perovskite solar cells.²² Zhang and Li synthesized pure anatase phase TiO_2 films on quartz glass, glass, gallium oxide-doped zinc oxide films (GZO) and p-type silicon substrates by mist CVD.²³ The TiO_2 films deposited on all substrates showed the same dominant (101) growth orientation. The crystallinity of the TiO_2 films increased depending on the type of substrate in the following order: glass, quartz glass, p-type silicon and GZO.²³ While the industrially important and mass-produced rutile phase of TiO_2 has been extensively studied in the past, compelling research has recently been conducted on the anatase phase of TiO_2 . Subsequent to conducting extensive electrical and optical spectroscopic studies, Tang et al. have concluded that anatase TiO_2 possesses very different electrical and optical properties compared with the better-known rutile phase of TiO_2 .²⁴ They reported that the electronic and optical properties of anatase TiO_2 films differ appreciably from the rutile phase with

only the anatase phase exhibiting an insulator–metal transition for high doping concentrations.²⁴ In the current study, we also find that the mechanical properties of the anatase TiO_2 films differ significantly from the mechanical properties of the rutile phase published elsewhere.²⁵ We employ the nanoindentation technique to investigate the mechanical properties of the ALD TiO_2 thin films. This technique offers an alternative to the conventional uniaxial tension or compression tests in the case of bulk samples and is traditionally used to investigate the mechanical properties of microscopic samples and thin films such as the ALD TiO_2 films in this study.

In the past, several deposition techniques have been used to deposit TiO_2 films onto silicon substrates including reactive DC sputtering,²⁰ RF magnetron sputtering,¹⁶ ion beam-induced chemical vapor deposition,²¹ metal–organic chemical vapor deposition MO-CVD,²⁶ chemical vapor deposition CVD,¹⁷ mist CVD²³ and the most recently developed atomic layer deposition (ALD) technology, which is the deposition technique that has been used in the synthesis of the TiO_2 films in the present study. ALD has emerged as a modern chemical reaction-based technique to deposit monolayers of inorganic compounds.^{27–34} ALD technology produces thin films with exceptional features such as precise thin film growth with atomic resolution, high uniformity, surface saturating property, self-limiting precursor reactions and superior film conformality even for extreme aspect ratio deposition. During ALD deposition and subsequent to the initial nucleation, the film thickness is linearly dependent on the number of ALD deposition cycles. A typical ALD cycle starts with exposing the substrate in the ALD reaction chamber to the first chemical ALD precursor followed by purging the chamber with inert gas (e.g., Ar, N_2) and finally exposing precursor-2 to the substrate, which reacts with precursor-1 to synthesize the desired final thin-film binary compound. This last step involves purging with N_2 , which removes the remaining unreacted precursor vapors through the vent using a vacuum pump.

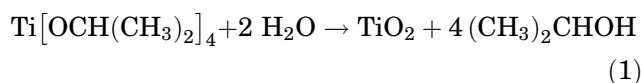
In this study we investigate the nanomechanical and structural properties of crystalline titanium dioxide (TiO_2) films of 500 nm thickness synthesized using atomic layer deposition (ALD) on p-type Si (100) substrates. The nanomechanical properties were measured using a nanoindenter equipped with a three-sided Berkovich diamond tip to evaluate the hardness and modulus of the TiO_2 thin films.

EXPERIMENTAL DETAILS

Film Deposition

TiO_2 films were deposited with angstrom resolution on 4-inch p-type poron Si (100) wafers covered with native oxide using thermal ALD synthesis technology utilizing a Veeco Nanotech Savannah 100 cross-flow ALD reactor. All ALD TiO_2 synthesis

experiments were carried out by thermal ALD in a cross-flow reactor design. Generally, 20 sccm N_2 was used as a carrier gas flow rate for the precursors. This carrier gas flow rate enabled proper transport of the chemical ALD precursors from the precursor cylinder into the ALD reaction chamber. The chamber base pressure was kept at 40 mTorr. The ALD TiO_2 thin-film depositions were performed at 250°C using alternate ALD deposition cycles of DI water vapor with a pulse duration of 0.015 s as the oxidant, which is followed by an ALD cycle with the organometallic alkoxide titanium isopropoxide with a pulse duration of 0.065 s as precursor-2. These alternating ALD deposition cycles are repeated n times until the desired TiO_2 film thickness has been achieved. Titanium isopropoxide, also known as titanium tetraisopropoxide or TTIP with the chemical formula $Ti[OCH(CH_3)_2]_4$, was heated to 75°C in a stainless steel container to achieve the correct vapor pressure for its release. The N_2 purging time was 5 s. The deposition rate was about 0.3–0.4 Å per ALD deposition cycle, at 250°C growth temperature. The final ALD synthesis of TiO_2 occurs by the reaction of titanium isopropoxide, with deionized water according to the chemical reaction equation:



During the ALD deposition process, the titanium isopropoxide reacts with the OH^- group to produce TiO_2 thin films, and the byproduct $(CH_3)_2CHOH$ is pumped out by the vacuum pump.

FILM CHARACTERIZATION

The structure of the films was examined using x-ray diffraction (XRD, with a MiniFlex II, from Rigaku, Japan, $CuK\alpha 1$ irradiation, $\lambda = 1.5406$ Å). The TiO_2 film thickness was verified using cross-sectional samples in a JEOL JSM-600LV FE-SEM at an accelerating voltage of 25 kV. The mechanical properties of the TiO_2 films were measured using a nanoindenter XP from Agilent Technologies, used in conjunction with the CSM (continuous stiffness method) in depth control mode. Using the CSM module allows the stiffness of contact and subsequently the mechanical properties of the sample to be constantly evaluated by analyzing the harmonic force and harmonic displacement data, as detailed elsewhere.³⁵ The nanoindenter XP is equipped with a three-sided diamond Berkovich probe. The Berkovich indenter tip was calibrated on fused silica standards for an initial indentation depth of 100 nm, 500 nm and 2 μm . The allowable drift rate and the strain rate were specified as 0.05 nm/s and 0.05/s, respectively.

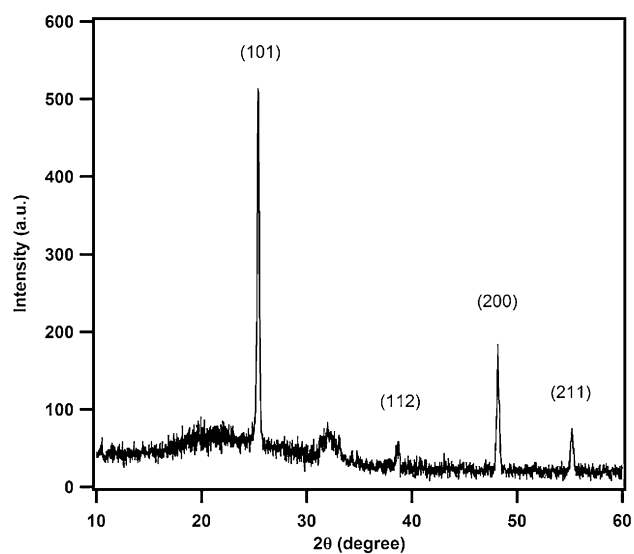


Fig. 1. XRD patterns of ALD TiO_2 thin films indicating that ALD synthesis at 250°C results in polycrystalline TiO_2 films with an anatase structure.

RESULTS AND DISCUSSION

XRD Results

Figure 1 depicts the XRD patterns of ALD TiO_2 thin films indicating that the ALD synthesis at 250°C resulted in polycrystalline TiO_2 films. The peaks in the XRD plot were indexed (JCPDS no. 21-1272) and fitted to pure anatase TiO_2 phases with significant peaks at (101) and (200) indicating dominant grain orientations. Therefore, using ALD technology, our samples revealed anatase phase with (101) and (200) dominant lattice planes. Jin et al. (2015) studied TiO_2 films deposited at different growth temperatures from 175°C to 400°C. For temperatures between 200°C and 250°C, the films show anatase crystal phase, with the (101) and (200) peaks in the x-ray diffraction patterns.³⁶ The intensity of the anatase (101) peak reaches a maximum at the growth temperature of 250°C and then decreases dramatically at a temperature above 300°C, with an emergence of a weak (110) peak from rutile TiO_2 . The results of the XRD of Fig. 1 showed that significant anatase TiO_2 peaks existed at (101) and (200), which are similar to those observed by Jin et al. (2015), indicating dominant grain orientations.³⁶ Therefore, using low temperature ALD technology at 250°C, our TiO_2 samples revealed exclusively pure anatase phase with (101) and (200) preferred dominant lattice orientation. The preferred grain orientation is attributed to internal surface stress and hydroxyl surface termination of our Si substrates used for ALD synthesis of TiO_2 . The difference between the ALD-grown TiO_2 thin films and those grown by conventional magnetron sputtering is that the columnar grains in the ALD TiO_2 thin films exhibited a more symmetrical distribution in the horizontal and vertical

directions (axis perpendicular to the substrate), whereas the columnar grains in the sputtered TiO_2 thin films grew preferentially larger along the vertical direction resulting in very thin elongated columnar structures giving rise to a higher grain boundary density.

FE-SEM and AFM Results

Figure 2 shows FE-SEM images of the ALD TiO_2 sample A and B films. According to the FE-SEM of Fig. 2, sample A is slightly thicker than sample B. By inspecting the FE-SEM images of Fig. 2, we noticed the formation of predominant symmetric columnar grains of the ALD TiO_2 thin films in the horizontal and vertical directions, which was also verified by the SEM and AFM images of Figs. 3 and 4. The ALD TiO_2 film thickness is ~ 500 nm, as indicated by Fig. 2. The polycrystalline morphology of the ALD films indicates a Volmer-Weber crystalline TiO_2 film growth mechanism by heterogeneous nucleation on the hydroxyl-terminated SiO_2 surface of the Si substrates. We observed that nucleation of islands was dominant over extended growth at layer edges of the TiO_2 from Fig. 2. This generally happens if the new precipitating species or atoms tend to cluster or strongly bond with each other rather than to the substrate surface. As a general rule in atomic layer deposition (ALD) technology, whenever the optimum ALD film deposition temperature exceeds the crystallization temperature of the specific compound, heterogeneous nucleation takes place following the Volmer-Weber island growth mode resulting in random polycrystalline films, which can include stress-induced preferred grain orientations, as in the case of ALD anatase TiO_2 .

Nanoindentation Results

To measure the elastic properties of the thin-film anatase TiO_2 samples, a Nanoindenter XP was used in conjunction with the continuous stiffness method

in depth control mode. The samples were tested at an indentation depth of 120 nm (24% of the film thickness) using the continuous stiffness method. The purpose of performing indentations of up to 24% of the film thickness is to measure the mechanical properties of the films and circumvent the substrate effects.

Figure 5 represents the hardness of the ALD TiO_2 films plotted versus contact depth of indentation (h_c) normalized to the film thickness (h_{film}). Figure 6 represents the modulus of the ALD TiO_2 films plotted versus the contact depth of indentation. Since we used the CSM module of the Nanoindenter XP to measure the mechanical properties of the ALD TiO_2 films, the CSM allows the stiffness of contact, and subsequently the mechanical properties of the sample, to be constantly evaluated by analyzing the harmonic force and harmonic displacement data. Therefore, from Fig. 5, given the film thickness, we could certainly back out the depth of indentation from the ratio of h_c/h_{film} . For example, for a ratio of h_c/h_{film} between 0.05 and 0.24, which corresponds to depths of indentation

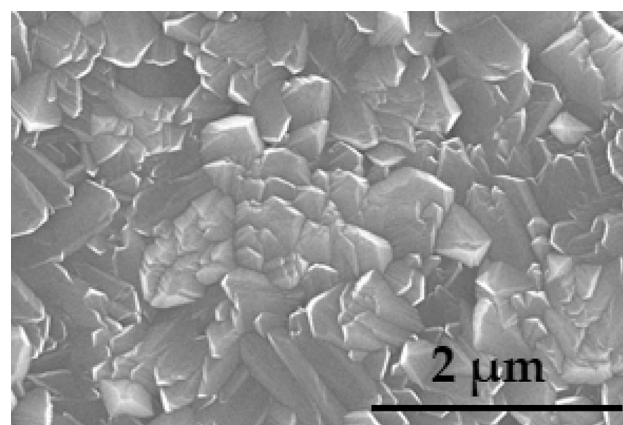


Fig. 3. Planar view FE-SEM micrograph of surface morphology of ALD synthesized anatase TiO_2 films.

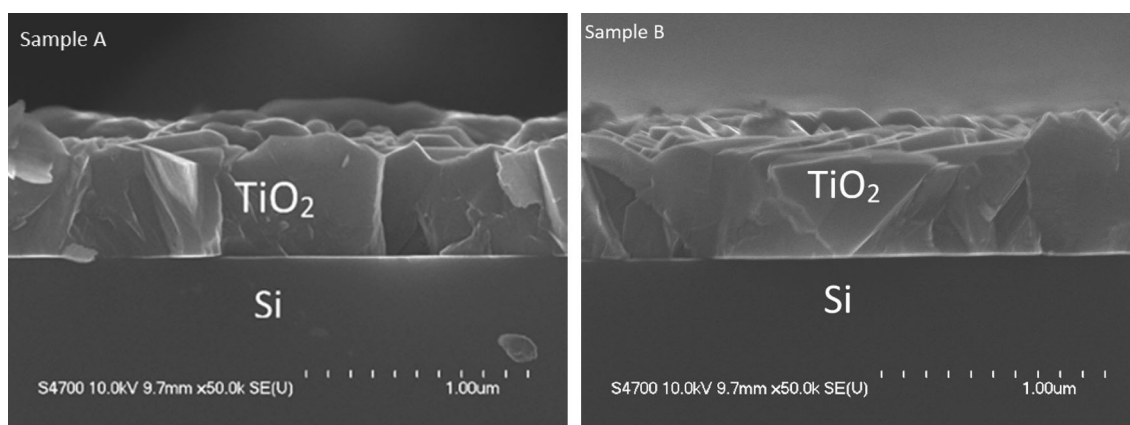


Fig. 2. FE-SEM cross-sectional images of ALD synthesized anatase TiO_2 films revealing columnar grain growth.

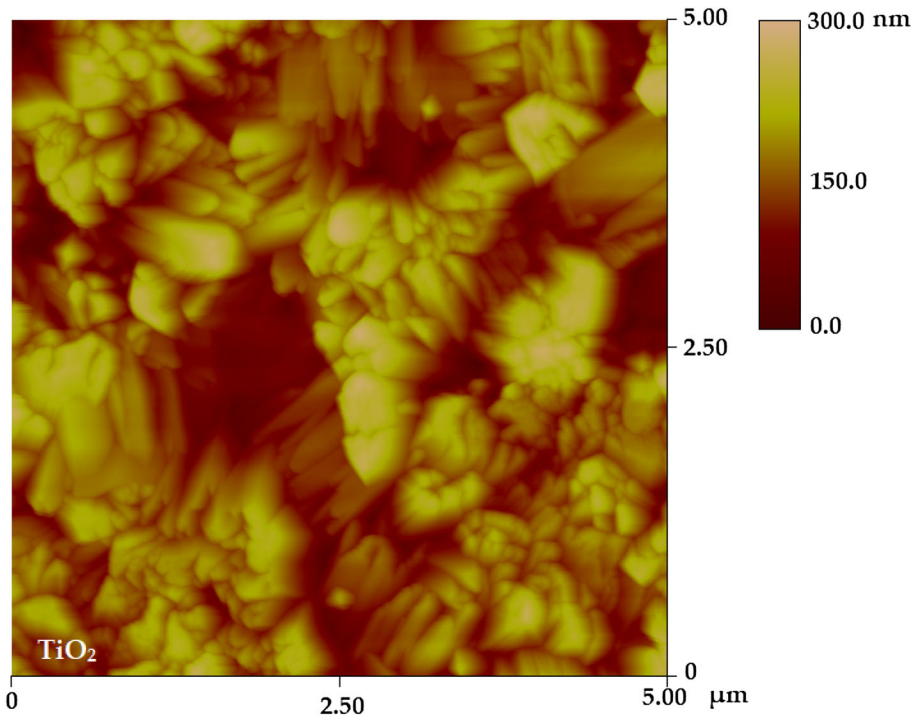


Fig. 4. AFM surface mapping image of ALD synthesized anatase TiO_2 films revealing columnar grains and surface roughness.

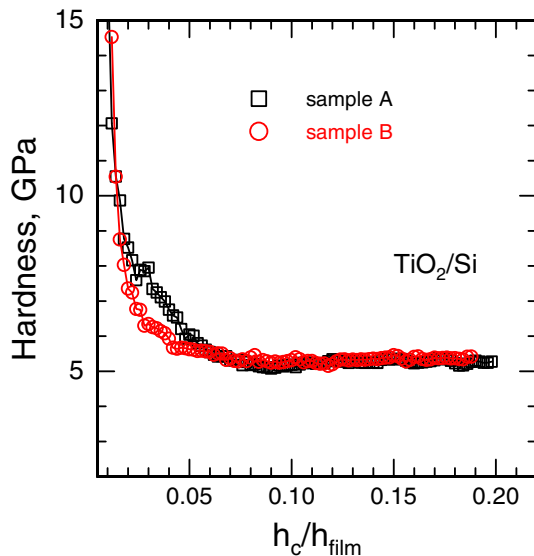


Fig. 5. Hardness versus indentation depth of the anatase phase of polycrystalline ALD TiO_2 samples synthesized by ALD technology.

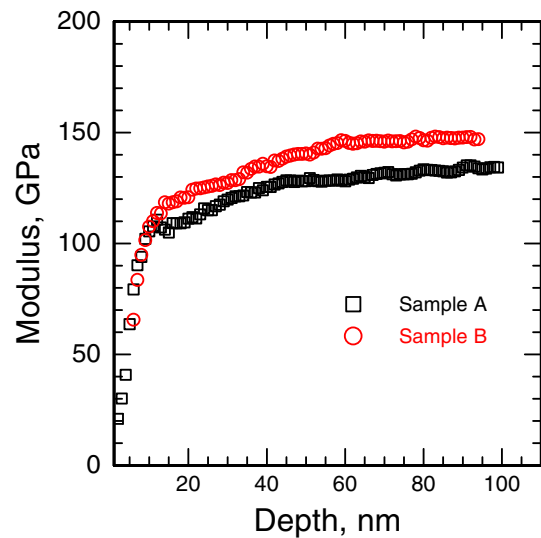


Fig. 6. Modulus versus indentation depth of the polycrystalline anatase ALD TiO_2 films of 500 nm thickness.

between 25 nm and 120 nm, the hardness is measured between 5.1 ± 1.7 GPa to 6.3 ± 1.6 GPa for both samples. If we consider the high end of the ratio of h_c/h_{film} , the measured hardness of the anatase ALD TiO_2 at 24% of the film thickness for samples A is $\sim 6.3 \pm 1.8$ GPa and 6.4 ± 1.7 for sample B. Similarly, the elastic moduli are $\sim 141.4 \pm 22.6$ GPa and 142.5 ± 29 GPa for samples A and B measured at 120 nm depth of indentation or 24%

of the film thickness, respectively. The hardness results for the anatase ALD TiO_2 thin films are similar to the hardness results of the single ALD anatase results of Testoni et al.³⁷ Lytinen et al.³⁸ noted that the hardness of the ALD TiO_2 samples deposited at 110–300°C increased with the deposition temperature probably because of phase transformation from amorphous film (110°C) to a mixture of amorphous/nanocrystalline anatase film (200°C) to fully crystalline anatase film (300°C). Lytinen

et al.³⁸ reported the hardness of the ALD TiO₂ film of 100 nm thickness deposited using TiCl₄/H₂O at a process temperature of 200°C as 8.5 GPa. Therefore, it is obvious that the hardness measurements of the anatase ALD TiO₂ films vary between 3.59 GPa and 8.5 GPa. The current results of the ALD TiO₂ anatase films are well within this range. Furthermore, Wojcieszak et al.¹⁸ obtained hardness results of ~ 4.8 GPa using the magnetron-sputtered TiO₂. However, Kaczmarek et al.³⁹ noted that low-pressure hot target reactive sputtering resulted in hardness of TiO₂ thin films of 3.5 GPa and 7.9 GPa for as-deposited and annealed films, respectively. Jouanny et al.²⁵ reported results for mixed anatase and rutile TiO₂ thin-film phases deposited by radiofrequency reactive sputtering in Ar-O₂ atmosphere on (100) silicon between ~ 5.9 GPa and 12 GPa for hardness and ~ 140 GPa to 193 GPa for modulus for samples #1 and #2, respectively. Samples #1 and #2 differ in the total pressure used with a total pressure of 1.47 Pa for sample #1 and a total pressure of 0.67 Pa for sample #2. Sample #1 x-ray diffraction revealed anatase and rutile diffraction peaks with the anatase as a dominant phase, whereas in sample #2 the corresponding x-ray diffractogram exhibited a mixture of rutile and anatase. Although these hardness and modulus results of sample #1 are comparable to the results we obtained in this research for a single-phase anatase ALD TiO₂ thin film, the hardness and modulus results of sample #2 are considerably above the average of a single anatase phase results. This suggests that the harder rutile phase in the mixed phases of sample #2 of Jouanny et al.²⁵ is dominant. In a study of TiO₂ films deposited by pulsed DC magnetron sputtering with various O₂:Ar ratios, Mazur⁴⁰ recognized that the change of sputtering gas atmosphere ratio strongly influenced the hardness of the TiO₂ coatings. He reported a hardness value of 10.5 GPa for anatase TiO₂ thin films deposited with an O₂:Ar ratio of 2:1 while a lowest value of 5.6 GPa for rutile TiO₂ coatings deposited with an O₂:Ar ratio of 1:2. However, Mazur⁴⁰ acknowledged that higher hardness values are usually observed in rutile structures. Villegas et al.⁴¹ reported similar hardness results to sample #2 of Jouanny et al.²⁵ of 10.7 GPa. Our measurements establish that the crystalline metastable low-temperature polymorph anatase TiO₂ film's mechanical properties represented by the hardness and modulus differ significantly from the harder and more robust rutile phase of Jouanny et al.²⁵ Our data also suggest that in addition to XRD, nanoindentation analysis can be used to differentiate between rutile and anatase or mixed phases TiO₂ films in a straightforward way. The results of the nanomechanical properties of the pure anatase phase TiO₂ ALD films complement the earlier reported findings of Tang et al.²⁶ that revealed significant differences in the electrical

and optical properties between anatase and the well-characterized rutile phase TiO₂.

CONCLUSION

We investigated the growth of crystalline TiO₂ films of 500 nm thickness on a Si substrate fabricated using low-temperature ALD deposition technology. The thickness of the TiO₂/Si film stack was verified by measuring the samples cross-sections using field emission scanning electron microscopy (FESEM). XRD analysis established that the ALD synthesis at 250°C of TiO₂ films resulted in the polycrystalline anatase phase with a largely symmetrical columnar grain structure growth in the horizontal and vertical directions resulting in roughly the same grain width as the grain height. This indicated that the ALD TiO₂ grain width is only limited by the film thickness, which needs to be benchmarked against the reported literature value of 12 GPa of pure rutile phase TiO₂. These reported findings constitute valid arguments for the measured softer mechanical properties of anatase ALD TiO₂ films in our nanoindentation study. For the application potential, recent literature reports have demonstrated that pure anatase phase TiO₂ thin films offer unique advantages in MOS thin-film gas sensors and photovoltaics for novel perovskite/heterojunction solar cells, which are attributed to the dominant (101) facets in anatase films.^{14,15}

REFERENCES

1. N. Huang, P. Yang, Y.X. Leng, J.Y. Cheng, H. Sun, J. Wang, G.J. Wang, P.D. Ding, T.F. Xi, and Y. Leng, *Biomaterials* 24, 2177 (2003).
2. U. Diebold, *Surf. Sci. Rep.* 48, 53 (2003).
3. A.S. Kumar, K.K. Nagaraja, N.M. Huang, and H.S. Nagaraja, *Mater. Lett.* 123, 149 (2014).
4. M.A. Mansoor, M. Mazhar, A. Pandikumar, H. Khaledi, H.N. Ming, and Z. Arifin, *Int. J. Hydrogen Energy* 41, 9267 (2016).
5. M. Dhayal, J. Jun, H.B. Gu, and K.H. Park, *J. Solid State Chem.* 180, 2696 (2007).
6. J. Domaradzki, D. Kaczmarek, E.L. Prociow, A. Borkowska, D. Schmeisser, and G. Beuckert, *Thin Solid Films* 513, 269 (2006).
7. M. Kadoshima, M. Hiratani, Y. Shimamoto, K. Torii, H. Miki, S. Kimura, and T. Nabatame, *Thin Solid Films* 424, 224 (2003).
8. N. Martin, D. Barette, and C. Rousselot, *J. Rauch. Surf. Coat. Technol.* 107, 172 (1998).
9. Z.M. Zeeley, A. Bandyopadhyay, and S. Bose, *Mat. Sci. Eng. B.* 164, 38 (2009).
10. O.K. Tan, W. Cao, W. Zhu, J.W. Chai, and J.S. Pan, *Sens. Actuators B* 396, 93 (2003).
11. A. Hazra, S. Das, J. Kanungo, C.K. Sarkar, and S. Basu, *Sens. Actuators B. Chem.* 183, 87 (2013).
12. Z.M. Zeeley, A. Bandyopadhyay, and S. Bose, *Thin Solid Films* 519, 434 (2010).
13. D. Mardare, N. Iftimie, and D. Luca, *J. Non-Cryst. Solids* 354, 4396 (2008).
14. E. Sennik, N. Kilinc, and Z.Z. Ozturk, *J. Alloys Compd.* 616, 89 (2014).
15. L. Etgar, P. Gao, Z. Xue, Q. Peng, A.K. Chandiran, B. Liu, MdK Nazeeruddin, and M. Graetzel, *J. Am. Chem. Soc.* 134, 17396 (2012).

16. N. Martin, C. Rousselot, D. Rondot, F. Palmينو, and R. Mercier, *Thin Solid Films* 300, 113 (1997).
17. K.S. Yeung and Y.W. Lam, *Thin Solid Film.* 109, 169 (1983).
18. D. Wojcieszak, M. Mazur, J. Indyka, A. Jurkowska, M. Kalisz, P. Domanowski, D. Kaczmarek, and J. Domaradzki, *Mater Sci-Poland* 33, 660 (2007).
19. M. Radecka, K. Zakrzewska, H. Czternastek, and T. Stapinski. *App. Surf. Sci.* 65/66 227 (1993).
20. P. Lobl, M. Huppertz, and D. Mergel, *Thin Solid Films* 251, 72 (1994).
21. D. Leinen, A. Fernandez, J.P. Espinos, T.R. Belderrain, and A.R. Gonzalez-Elipse, *Thin Solid Films.* 241, 198 (1994).
22. S. Alimirsalari, F. Tajabadi, S.M. Salehkoutahi, R. Ghahary, and N. Taghavinia, *RSC Adv.* 4, 45174 (2014).
23. Q. Zhang and C. Li, *ECS J. Solid. State. SC.* 7, P654 (2018).
24. H. Tang, K. Prasad, R. Sanjines, P.E. Schmid, and F. Levy, *J. Appl. Phys.* 75, 2042 (1994).
25. I. Jouanny, S. Labdi, P. Aubert, C. Buscema, O. Maciejak, M.-H. Berger, V. Guipont, and M. Jeandin, *Thin Solid Films* 518, 3212 (2010).
26. G. Battison, R. Gerbasi, and M. Porchia, *Thin Solid Film.* 239, 186 (1994).
27. J. Aarik, A. Aidla, T. Uustare, M. Ritala, and M. Leskelä, *Appl. Surf. Sci.* 161, 385 (2000).
28. S. Zhuiykov, M.K. Akbari, Z. Hai, C. Xue, H. Xu, and L. Hyde, *Data in Brief.* 13, 401 (2017).
29. Z. Insepov, A. Ainabayev, F. Bozheyev, A. Zhuldassov, M. Lukasheva, and K.B. Tynyshtybaev, *Mater. Today* 4, 11630 (2017).
30. A.P. Alekhin, S.A. Gudkova, A.M. Markeev, A.S. Mitiaev, A.A. Sigarev, and V.F. Toknova, *App. Surf. Sci.* 257, 186 (2010).
31. R. Hussin, K.L. Choy, and X. Hou, *APRN J. Eng. Appl. Sci.* 11, 7529 (2016).
32. A. R. Head, N. Johansson, Y. Niu, O. Snezhkova, S. Chaudhary, J. Schnadt, H. Bluhm, C. Chen, J. Ávila, and M.-C. Asensio. *J. Vac. Sci. Technol. A.* 36 02D405 1 (2018).
33. M. Ritala, M. Leskelä, L. Niinisto, and P. Haussalo, *Chem. Mater.* 5, 1174 (1993).
34. M. Aghaee, J. Verheijen, A.A.E. Stevens, E. Kessels, and A. Creatore, *Plasma. Process. Polym.* 16, 1 (2019).
35. W.C. Oliver and G.M. Pharr, *J. Mater. Res.* 19, 3 (2004).
36. C. Jin, B. Liu, Z. Lei, and J. Sun, *Nanoscale Res. Lett.* 10, 95 (2015).
37. G.E. Testoni, W. Chiappim, R.S. Pessoa, M.A. Fraga, W. Miyakawa, K.K. Sakane, N.K.A.M. Galvão, L. Vieira, and H.S. Maciel, *J. Phys. D Appl. Phys.* 49, 375301 (2016).
38. J. Lyytinen, X. Liu, O.E.Y. Livaara, S. Sintonen, A. Lyer, S. Ali, J. Julin, H. Lipsanen, T. Sajavaara, R.L. Puurunen, and J. Koskinen, *Wear.* 342-343, 270 (2015).
39. D. Kaczmarek, J. Domaradzki, D. Wojcieszak, E. Prociow, M. Mazur, F. Placido, and S. Lapp, *J. Nano Res.* 18–19, 195 (2012).
40. M. Mazur, *Opt. Mater.* 69, 96 (2017).
41. E.A. Villegas, R. Parra, and L. Ranahjo, *J. Mater. Sci. Mater. EL.* 30, 1360 (2019).

Publisher's Note Springer Nature remains neutral with regard to jurisdictional claims in published maps and institutional affiliations.